Journal of South American Earth Sciences 86 (2018) 461–474

Contents lists available at ScienceDirect

Journal of South American Earth Sciences

journal homepage: www.elsevier.com/locate/jsames

Petrology, geochemistry and U-Pb zircon and baddeleyite ages of the alkaline rocks from the central-southern Guyana Shield, northern Amazonian Craton

Raisa Fagundes de Figueiredo*, Ticiano José Saraiva dos Santos, Erica Martini Tonetto

Institute of Geosciences, University of Campinas, Brazil

ARTICLE INFO

Keywords:
Amazonian craton
Zircon and baddeleyite ages
Mesozoic alkaline magmatism
Phonolites
Syenites
Tacutu basin

ABSTRACT

The Apiaú Alkaline Complex (AAC) represents a rift-related intracontinental magmatism and occurs as intrusions within the Precambrian basement of the central-southern portion of the Guyana Shield, Amazonian Craton. The complex extends for over 200 km and comprises monzonites, syenites, nepheline syenites, nepheline-bearing syenites, trachytes and phonolites. It differs from other alkaline rocks of the craton both in age and tectonic setting. Here we report new petrologic, geochemical, and zircon and baddeleyite U-Pb geochronological information on the nepheline-bearing syenites and phonolites to discuss the petrogenetic and tectonic evolution of the AAC. Our new bulk rock major and trace elements analyses show that the complex is predominantly miaskitic, with potassic and sodic affinity, strong enrichment in light REE and negative Eu, Ba, Sr, P, and Ti anomalies. The phonolites and syenites geochemistry suggests similar fractionation processes from closely related parental melts for their genesis. Zircon and baddeleyite U-Pb crystallization ages of 111 ± 1 Ma and 116 ± 3, respectively, indicate a relationship between the alkaline magmatism and the opening of the Equatorial Atlantic Ocean. The spatial disposition of the alkaline rocks following major faults of the Amazonian Craton denotes a structurally controlled emplacement history by reactivation of ancient weakness zones. Crystallization ages are coincident with the Tacutu basin filling, evidencing a relative tectonic stability period and suggesting that the progressive subsidence contributed to the reactivation of the main structures in the region. The presence of inherited zircon from the orthoderived granitic basement (U-Pb ages of 1931 ± 4 Ma and 1958 ± 7 Ma) in a nepheline-bearing syenite, addition to petrography features and geochemical behaviour indicate that the alkaline magma was contaminated with Precambrian crustal rocks.

1. Introduction

Alkaline magmatism may occur in several tectonic settings, ranging from intraplate rifting to subduction zones (Fitton and Upton, 1987; Pirajno, 2015; Pagano et al., 2016). However, intracontinental alkaline complexes are generally associated with rifting because of local migration of volatiles from the asthenosphere that results in metasomatism of the lithospheric mantle and partial fusion of host rocks (Pirajno, 2015). In this context, the lithospheric architecture will influence either the locus of intraplate magmatism or the transport of fluids and deep magmas (Bailey, 1977; Begg et al., 2009).

The Brazilian platform is marked by alkaline and alkaline-carbonatitic complexes of different ages. The majority of them are Mesozoic to Cenozoic and cluster around important lineaments of the Paraná basin (Ulbrich and Gomes, 1981; Morbidelli et al., 1995; Gomes and Comin-Chiaramonti, 2005). For the Amazonian Craton, around 20 alkaline complexes have been described and occur as minor plutons along shear zones related to intracontinental extension (Cordani et al., 2010), most of them are Meso and Neoproterozoic (Teixeira, 1978; Ulbrich and Gomes, 1981; Gomes et al., 1990; Tassinari, 1996; Biondi, 2005).

The post-Paleozoic magmatism in Brazil has been associated with the occurrence of deep-seated fault systems in the basement and with the Gondwana break-up (Almeida, 1986). The alkaline rocks record a broad age interval, which Riccomini et al. (2005) consider that it took place in four stages under different stress-field, associated with the evolution of Atlantic Margin and continental rift systems. However, Gibson et al. (1995) propose that the Late Cretaceous alkaline magmatism in SE Brazil is related to Trindade mantle plume. Plate margin stresses and lithospheric extension associated with opening of the South Atlantic may also have changed the geothermal gradient and

* Corresponding author.
E-mail address: raisaffigueiredo@gmail.com (R.F.d. Figueiredo).

https://doi.org/10.1016/j.jsames.2018.08.001
Received 17 January 2018; Received in revised form 12 May 2018; Accepted 1 August 2018
Available online 03 August 2018
0895-9811/

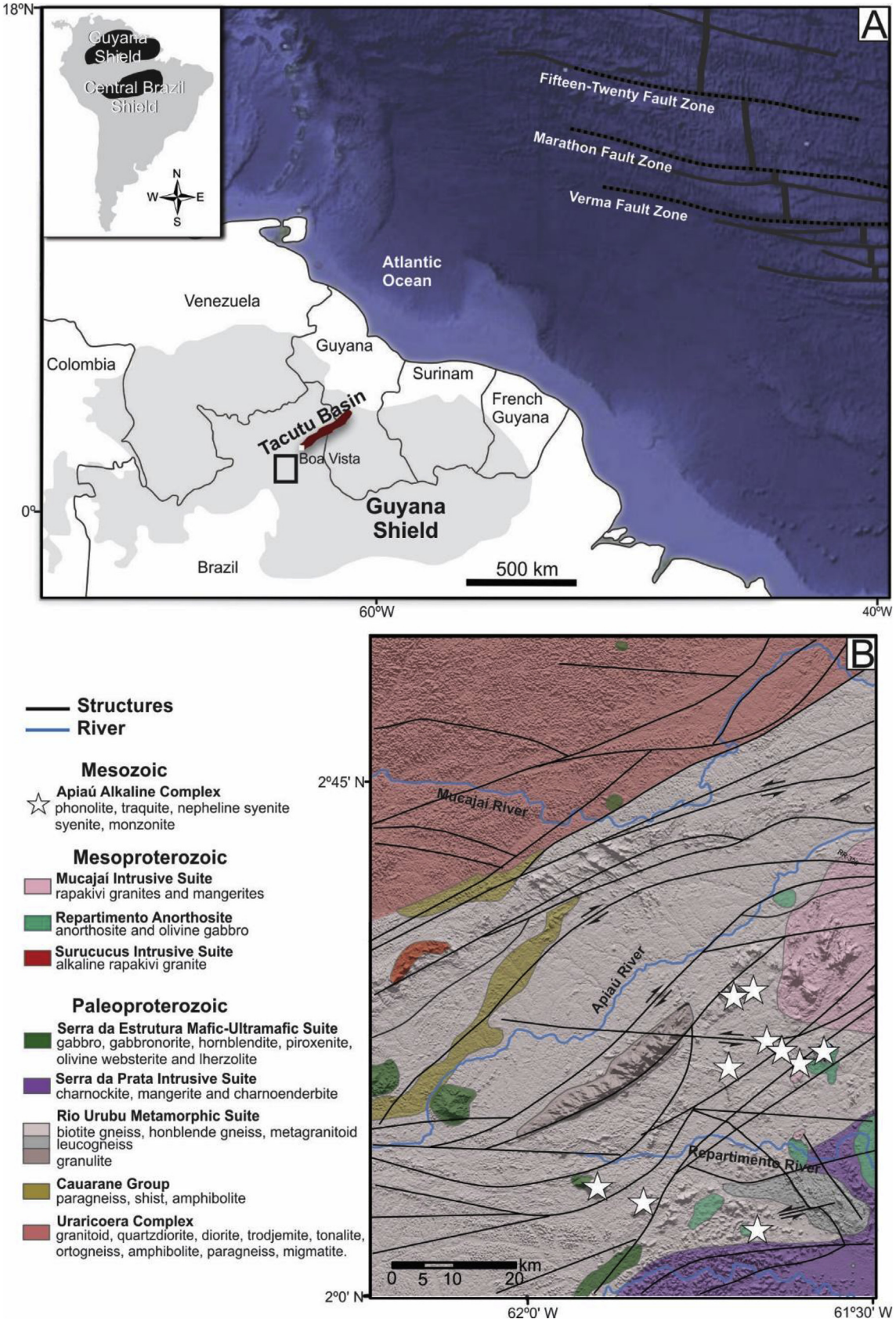

Fig. 1. A) Sketch map of the Amazonian Craton (dark gray) and Guyana Shield, showing the rift-related Tacutu basin (red). B) Geological map of the central-southern portion of the Guyana Shield (modified after Reis et al., 2004), with the distribution of alkaline rocks and their relationship with major structural features. (For interpretation of the references to color in this figure legend, the reader is referred to the Web version of this article.)

contributed to mantle melting (Gibson et al., 1999).

During the opening of the Atlantic Ocean, important structures of the Guyana Shield, in the Amazonian Craton, were reactivated and the intraplate extension led to the development of the Tacutu rift. This elongated NE-SW aulacogen basin located in the Guyana and Roraima state, started opening around 200 Ma (Marzoli et al., 1999; Leal et al., 2000; Reis et al., 2004, 2006) being marked by the presence of tholeiitic dykes, and filling during Early Cretaceous (Eiras and Kinoshita, 1988, 1990; Vaz et al., 2007). Concomitantly to the formation of the basin, alkaline magmatism represented by the Apiaú Alkaline Complex (AAC) took place in the Brazilian northernmost portion (Salas and Santos, 1974; Montalvão et al., 1975; Figueiredo, 2016).

Previous studies conducted by Montalvão et al. (1975) established a Rb/Sr whole-rock age of 100 Ma for the AAC nepheline syenite. Nevertheless, the lack of robust geochronological and geochemical data for the Amazonian alkaline rocks has hampered the comprehension of the geological and geotectonic processes responsible for the ascension of the alkaline magma. In order to better understand such magmatism, we combined petrographic and geochemical data with precisely AAC crystallization dating, zircon and baddeleyite U-Th-Pb methods, to determine the geodynamic context in which these rocks were generated.

2. Geological setting

The Apiaú Alkaline Complex (AAC) is located in the Guyana Shield, north of the Tapajós-Parima (Santos et al., 2000, 2006a) or Ventuari-Tapajós Province (Tassinari and Macambira, 1999, 2004). This geochronological province is considered a Paleoproterozoic (2.03–1.88 Ga) orogenic belt, composed of granulitic/gneiss-migmatitic terrains and metavolcanic and metasedimentary units deformed and metamorphosed to the greenschist to amphibolite facies (CPRM, 1999; Fraga, 2002; Tassinari and Macambira, 2004; Reis et al., 2004; Almeida, 2006).

The region where the alkaline rocks occur is structurally complex; it is embedded in the Central Guyana Domain (CGD) that crosses the Guyana Shield, from Suriname, passing through Guyana and ending in Brazil (Roraima and Amazonas states). The CGD is composed predominantly of amphibolite-to granulite-facies orthogneisses with ages between 1.96 and 1.91 Ga (Gaudette et al., 1996; Fraga et al., 1997; Fraga, 2002; Reis et al., 2003) metamorphosed at 1.91 Ga (Costa, 2005). Anorthosite/gabbro-mangerite-granite rapakivi associations dating ca. 1.5 Ga intrude CGD (Gaudette et al., 1996; Fraga, 2002; Reis et al., 2003; Fraga et al., 2009; Heinonen et al., 2012). On the southeastern limit of CGD, mylonites and foliated granites associated with broad NE-SW shear zones are related to the Itã event with ages around 1.72 Ga (Almeida, 2006; Almeida et al., 2008). Between 1.49 and 1.15 Ga there is the record of the K'Mudku event, in which mylonites of low metamorphic grade and intraplate magmatism were generated (Santos et al., 2000, 2006b; 2009; Fraga, 2002; Fraga et al., 2009; Cordani et al., 2010; Souza et al., 2015).

The tectonic events that took place in the Guyana Shield developed major weakness zones that were reactivated during the break-up of Gondwana, generating magmatism and intracontinental rifting. The Tacutu basin corresponds to an aulacogen in the central part of the Guyana Shield, related to the opening of the Atlantic Ocean in parts of Brazil and Guyana (Vaz et al., 2007). Seismic sections indicate an asymmetric hemi-graben structure reaching seven thousand meters in thickness (Eiras and Kinoshita, 1988, 1990; Vaz et al., 2007). The general architecture of the Tacutu basin is represented by a pack of NE-SW normal faults that follow the basement mylonitic zone trend, in addition to NW-SE strike-slip faults (Costa et al., 1991).

The initial rift phase of the Tacutu basin is marked by tholeiitic magmatism of the Central Atlantic Magmatic Province - CAMP (represented by the Apoteri Formation), with the establishment of dykes around 200 Ma and volcanic floods between 153 and 135 Ma (Marzoli et al., 1999; Leal et al., 2000; Reis et al., 2004, 2006). The filling of the basin occurred during the Early Cretaceous with the sedimentation of the sandstones of Serra do Tucano Formation (Eiras and Kinoshita, 1988, 1990; Vaz et al., 2007). However, the relative stability of the basin was interrupted by a transpressive event during the Miocene/Pleistocene that resulted in the deposition of the Boa Vista Formation that extrapolates the limits of the graben (Eiras and Kinoshita, 1988).

The AAC is located in the central-southern portion of the Guyana Shield, Amazonian Craton (Fig. 1). It comprises monzonite, syenite, nepheline-bearing syenite and nepheline syenite bodies of hundreds of meters to 5 km in extension, plus trachytes and phonolites dykes (Salas and Santos, 1974; Montalvão et al., 1975; Borges, 1990; Brandão and Freitas, 1994; CPRM, 1999; Figueiredo, 2016). These rocks are isotropic, with no evidence of metamorphism or ductile deformation, and are embedded in the orthogneiss terrains (Rio Urubu Metamorphic Suite), the gabbro-anorthositic sequence (Repartimento Anorthosite) and the rapakivi granites (Mucajaí Intrusive Suite) of Paleoproterozoic and Mesoproterozoic ages.

The alkaline rocks crop out in the southwestern prolongation of the Tacutu basin along important Precambrian lineaments. Nepheline syenite Rb-Sr ages point to a Cretaceous magmatism around 100 Ma (Montalvão et al., 1975), correlated with the extensional stress due to the opening of the Atlantic and the intracontinental rifting (Tacutu Basin). The main distribution of the occurrences is presented in Fig. 1.

3. Analytical methods

Geochemical analyses were performed at the Analytical Geochemical Laboratory of the Geosciences Institute of the University of Campinas. Major elements were determined by XRF (Philips, PW2404) according to the procedures described in Vendemiatto and Enzweiler (2001), using glass disks and pressed tablets. REE and other trace elements were determined by ICP-Q-MS (equipped with a collision cell) according to Cotta and Enzweiler (2011).

Three samples were selected for LA-ICP-MS determination of U-Th-Pb crystallization ages for AAC and its basement. The samples were crushed, milled and sieved to concentrate zircon; baddeleyite separation was performed according to the procedures described by Söderlund and Johansson (2002). Zircon and baddeleyite crystals were manually handpicked from the concentrates. The most transparent grains as much devoid of fractures, inclusions and imperfections as possible were mounted in epoxy resin and polished to a flat surface. Whereas zircons were polished to their equatorial cross sections, baddeleyite grains were just exposed from the resin. CL images of the zircon crystals were obtained with a Chroma CL – Gatan detector installed in a LEO 430i scanning electron microscope.

The zircon ages were obtained at the Isotope Geology Laboratory at the University of Campinas by LA-SF-ICP-MS, in a Thermo Scientific Element XR coupled with an Excite 193 laser ablation system from Photon Machines (spot diameter 25 µm, 91500 zircon as reference material and Peixe zircon as internal standard) according to the procedure stablished by Navarro et al. (2015). Baddeleyite ages were performed at the University of Stockholm by LA-Q-ICP-MS, in a 72 Thermo XSeries2 equipment coupled with an Excimer ESI-NWR 193 laser ablation system according to the described in Wohlgemuth-Ueberwasser et al. (2015) (spot 25 µm, FC-4b Duluth Gabbro baddeleyite as reference material and Phalaborwa baddeleyite as internal standard).

4. Petrographic features

4.1. Nepheline-bearing syenites

The nepheline-bearing syenites vary from nepheline-bearing syenite to nepheline-bearing alkali feldspar syenite. They are leucocratic until hololeucocratic, with grayish-whitish tints and inequigranular medium grain size. These macroscopic characteristics vary according to the

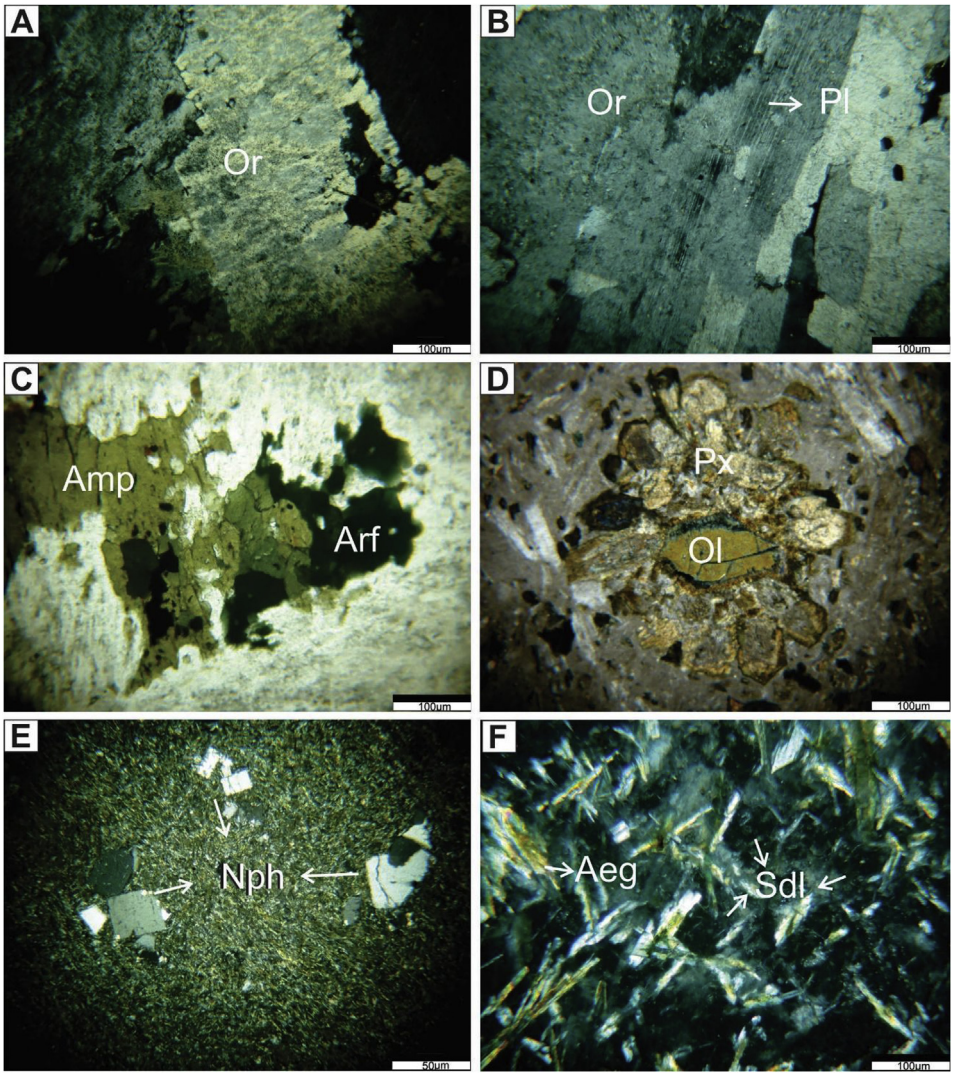

Fig. 2. Macro and microscopic features of nepheline-bearing syenites. A) Mesoperthitic orthoclase; B) Plagioclase replaced by orthoclase; C) Arfvedsonite partially altered by calcic amphibole. D) Olivine and pyroxene xenocrysts wrapped with amphibole E) Clustered euhedral grains of nepheline. F) Granular sodalite crystals dispersed in a clinopyroxene-rich matrix. Or-orthoclase; Pl-Plagioclase; Amp- Calcic amphibole; Arf-arfvedsonite; Px-pyroxene; Ol-olivine; Nph-nepheline; Sdl-sodalite.

contents of mafic minerals, which are higher in the nepheline syenite (23% modally), and interaction with magmatic fluids, which was more intense in the alkali feldspar syenite. Essential minerals are nepheline, alkali feldspar, oligoclase, calcic amphibole, arfvedsonite, and biotite. Accessories are represented by titanite, apatite, allanite, zircon, iron oxides and sulfides.

Orthoclase is the dominant alkali feldspar. It occurs in the form of anhedral to subhedral crystals, most of which with simple twinning and generally exhibiting cryptoperthites and patch perthites in the alkali feldspar syenite (Fig. 2A). Commonly orthoclase substitutes for oligoclase (Fig. 2B). Sericitization of orthoclase is frequent along cleavage and twining plains. Plagioclase occur locally as cumulate. The rare high Ca-plagioclase crystals are totally saussuritized. Oligoclase with subtle polysynthetic twinning occurs subordinately.

The main mafic mineral of the nepheline syenite is calcic amphibole. The crystals are generally elongated and subhedral, and sometimes anhedral, fragmented, exhibiting twinning; biotite and apatite inclusions are frequent. Uralitization is very common with an augite core. Arfvedsonite is subordinate and occurs as small fragments or as interstitial crystals to alkali feldspar, partially altered by calcic amphibole (Fig. 2C). Aggregates of calcic and sodic amphiboles occur locally. Biotite forms small subhedral inclusions or as elongated subhedral crystals with sericitized rims. Biotite is rare in the alkali feldspar syenite and shows altered rims.

Nepheline is the predominant feldspathoid and occurs either as euhedral crystals with hexagonal to rectangular polygonal sections intergrown with K-feldspar or as anhedral crystals or included in the biotite, pyroxenes and amphiboles. Occasionally, nepheline is replaced by cancrinite and sericite.

Apatite is the main accessory and occurs as hexagonal, rectangular or acicular euhedral crystals of varied grain sizes and also as inclusions in most minerals. Subordinate, titanite composes agglomerates of small euhedral crystals. Other accessory minerals are allanite, iron oxides, sulfides and rare subhedral zircon crystals.

4.2. Phonolites

These rocks vary from green to dark grey; and from massive to trachytic texture. The rock groundmass is very fine to aphanitic, sometimes microporphyritic to porphyritic and amygdaloidal. Where the groundmass is thicker, it is possible to recognize aegirine, augite, nepheline, sanidine and rarely diopside. The groundmass of some phonolites is composed essentially of augite and aegirine needles, occasionally disposed radially.

Table 1
Whole rock compositions of rocks from the AAC. Major elements in percentage (%) and trace elements in parts per million (ppm).

Lithotypes	Phonolite	Phonolite	Phonolite	Phonolite	Phonolite	Syenite	Syenite	Syenite
	Miaskitic	Miaskitic	Miaskitic	Agpaitic	Agpaitic			
Sample	RRTJ-12	RRTJ-13	RRTJ-30B	RRTJ-08	RRTJ-18	RRTJ-21	RRTJ-22	RRTJ-23
wt.%								
SiO_2	56.41	56.13	57.09	54.53	53.95	56.25	62.5	57.95
TiO_2	0.077	0.09	0.264	0.102	0.143	0.641	0.09	0.447
Al_2O_3	20.29	20.02	19.22	20.58	20.38	19.85	18.77	18.57
Fe_2O_3	4.38	4.6	4.12	3.13	4.01	5.75	3.6	5.99
MnO	0.218	0.217	0.149	0.238	0.22	0.123	0.202	0.22
MgO	0.06	0.1	0.85	0.01	0.04	1.24	0.16	1.16
CaO	1.12	1.33	1.84	0.91	1.21	3.86	1.25	3.36
Na_2O	8.5	7.45	7.53	11.2	10.31	5.94	6.85	5.91
K_2O	5.95	6.35	5.37	4.78	5.94	5.01	6.3	5.64
P_2O_5	0.066	0.059	0.141	0.036	0.03	0.465	0.047	0.339
LOI	2.9	3.63	3.4	4.19	3.84	0.46	0.46	0.62
Total	100	100	100	99.7	100.1	99.6	100.2	100.2
ppm								
Li	48.2	36	65.1	294	47.8	34.9	32.6	34.8
Be	7.33	6.62	10.1	13.3	9.95	2.93	4.54	3.01
Sc	0.92	0.86	2.39	1.62	1.19	1.87	1.04	2.25
V	1.25	1.14	14.6	2.44	1.42	40.6	2.05	36.9
Cr	4.27	3.81	12.6	5.21	3.11	6.65	7.52	7.61
Co	1.03	1.23	4.81	0.34	1.07	9.71	1.34	7.42
Ni	0.17	0.19	12	0.31	0.25	4.25	1.01	1.3
Cu	3.28	4.45	6.19	0.78	4.42	8.62	1.49	5.21
Zn	101	99.6	106	190	161	66.4	67.1	95.8
Ga	23.6	23	23.9	32.4	29.2	17.5	19.6	18
Rb	247	260	237	345	331	80.8	236	89
Sr	2.79	17.7	126	32.7	48	1206	90.4	518
Y	10.5	15.4	21.4	30.5	18.4	19.7	17.3	25.9
Zr	774	708	745	1218	998	315	748	697
Nb	273	273	214	543	343	170	237	215
Mo	6.1	4.12	6.76	9	10.5	3.22	2.66	2.06
Cd	0.21	0.19	0.2	0.44	0.28	0.11	0.17	0.15
Sn	2.47	2.5	2.99	3.04	2.41	1.26	1.64	1.83
Sb	0.37	0.38	0.53	1.09	0.61	0.14	0.41	0.23
Cs	3.7	8.1	12.7	9.86	7.84	2.3	3.46	2.17
Ba	2.61	27.7	125	18.3	18	3580	167	1525
La	49.4	104	120	91.8	149	142	110	137
Ce	151	144	165	205	231	194	170	212
Pr	6.17	13.2	13.9	8.69	16.1	18.8	16.9	23.2
Nd	16	35.1	36.1	20.5	40.6	55	47.5	68.8
Sm	1.92	3.92	4.66	2.83	4.58	6.66	5.52	8.61
Eu	0.16	0.37	0.6	0.63	0.8	2.63	0.46	1.82
Gd	2.18	3.75	4.8	3.5	4.72	6.26	4.93	7.38
Tb	0.25	0.44	0.62	0.54	0.52	0.72	0.59	0.89
Dy	1.51	2.58	3.7	3.86	2.94	3.75	3.34	4.94
Ho	0.35	0.58	0.8	0.96	0.67	0.74	0.7	1
Er	1.17	1.81	2.44	3.24	2.09	2.06	2.07	2.86
Tm	0.21	0.32	0.43	0.61	0.38	0.32	0.34	0.45
Yb	1.68	2.25	2.93	4.19	2.61	2.1	2.38	3.09
Lu	0.29	0.38	0.47	0.62	0.42	0.34	0.42	0.53
Hf	11.9	11.1	12	16.3	14.2	5.34	12.3	11.5
Ta	13.2	12.1	11.8	26.6	14.9	6.13	10	8.76
W	1.82	2.46	5.69	5.36	3.75	1.93	3.22	1.77
Pb	29.1	24.6	41.4	67.8	50.2	17.1	19.5	20.6
Bi	0.25	0.25	0.4	0.41	0.31	0.05	0.13	0.11
Th	20.5	29.5	67.2	25.7	43.7	16	26	19
U	9.77	8.27	16	18.4	22.8	4.01	5.7	4.53
(Eu/Eu*)	0.24	0.29	0.38	0.61	0.52	1.25	0.27	0.70
(La/Yb)CN	19.85	31.10	27.59	14.77	38.48	45.73	31.27	29.96
(La/Sm)CN	16.20	16.62	16.17	20.45	20.48	13.43	12.58	10.02
(Eu/Yb)CN	0.27	0.46	0.58	0.43	0.87	3.57	0.55	1.68
Ne*	19,909	15,985	12,703	29,094	30,500	5229	3982	4897
Or*	35,163	37,527	31,735	28,248	35,104	29,608	37,231	33,331
Ab*	34,485	33,532	40,268	25,536	15,453	40,610	50,612	40,970
An*	0.000	2430	2782	0.000	0.000	12,702	1860	7483

*Normative minerals CIPW.

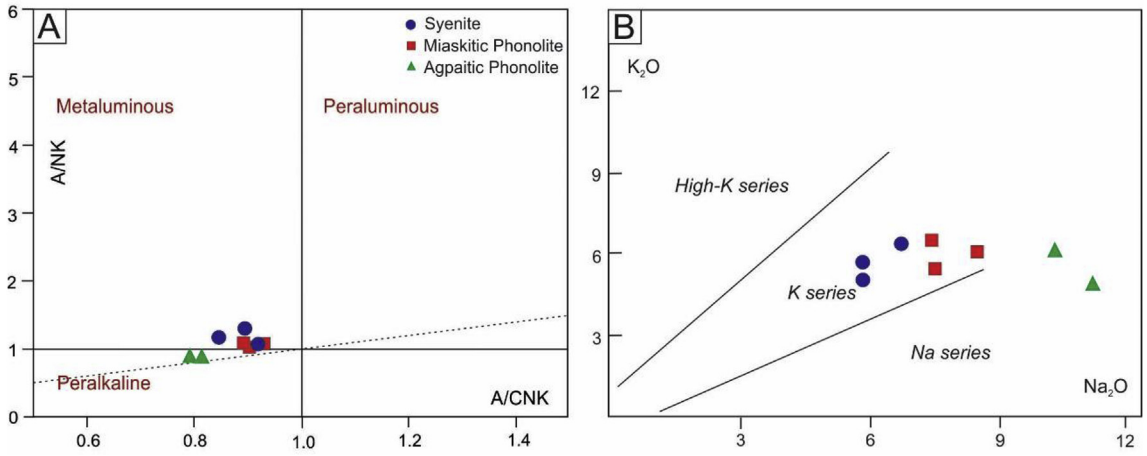

Fig. 3. Geochemical variation diagrams for the AAC phonolites and syenites. (A) Alumina saturation diagram (Shand, 1943) showing a peralkaline tendency for the majority of the AAC rocks. (B) High-potassic, potassic and sodic series diagram (Middlemost, 1975). Note the predominance of AAC rocks in the potassic series and the sodic tendency of the agpaitic phonolites.

The phonolites present phenocrysts/microphenocrysts of euhedral sanidine and nepheline, calcic amphibole, augite, and aegirine. Sanidine and nepheline are the most abundant phenocrysts and locally form glomeroporphyritic aggregates. Sanidine occurs as euhedral to subhedral prisms with Carlsbad twinning. The nepheline phenocrysts are euhedral occurring isolated or as clustered grains (Fig. 2E), and sometimes are totally or partially replaced by cancrinite. Cancrinite can also be a primary mineral scattered in the matrix, together with granular sodalite crystals (Fig. 2F). Aegirine phenocrysts are rare and were observed in only one sample.

One of the samples has olivine and pyroxene xenocrysts wrapped with amphibole, isolated from the groundmass (Fig. 2D). Two samples present eudialyte associated with zircon, which is characteristic of an agpaitic assembly. Thorite and fluorides, such as cryolite, are common. Besides, amygdales are filled up with aegirine, nepheline, fluorite and REE carbonates.

5. Geochemistry

The AAC rocks are silica unsaturated felsic rocks (Table 1). In the alkalinity diagram (Fig. 3A) from Shand (1943), the samples plot in the peralkaline or in the metaluminous field, next to the peralkaline field. Some phonolites are classified according to the alkalinity index as peralkaline, whereas the syenites are metaluminous, but tend to the peralkaline field. Two phonolite samples are agpaitic for the presence of eudialyte (Le Maitre, 2002). The majority of the rocks are potassic (Fig. 3B), except for the peralkaline phonolites, which fall in the sodic series, as shown in the K_2O vs Na_2O diagrams (Middlemost, 1975). The rocks have low compatible element contents, such as Ni, Cr and Co, except for a phonolite sample that has significantly higher Cr and Ni contents and syenite samples with high Co contents. Major and trace elements contents are presented in Table 1.

Incompatible elements normalized to primitive mantle (McDonough and Sun, 1995) show mild difference between syenite and phonolite patterns (Fig. 4A). In spite of the similar enrichment patterns, their intensities are far distinct. The phonolites are characterized by intense negative anomalies of Ba, Sr, P and Ti, whereas only one syenite sample show intense anomalies. Besides that, the agpaitic phonolites are more enriched in U, Pb and Zr than others rocks from AAC.

On chondrite-normalized plots (Boynton, 1984), the rocks are all enriched in REE when compared to chondrite REE concentrations. The majority of the rocks show strong LREE enrichments, with $[La/Yb]_{CN}$ between 15 and 46. LREE are 100–400 times and HREE approximately 10 times chondrite (Fig. 4B). The syenites tend to be enriched MREE than all other rocks, and presenting both small negative and positive Eu anomalies. In general, the Eu/Eu* ratios for AAC have wide variation (0.24–1.25), although in most of them the anomalies are negative. For the agpaitic phonolite dykes, the Eu/Eu* ratios have smallest variation, with values of 0.52 and 0.61, whereas for syenites this ratio ranges from 0.27 to 1.25.

One syenite sample differ by having significantly higher Ba, Sr and Eu contents than all other rocks. The wide ranges in Ba (167–3580 ppm), Sr (90.4–1206 ppm), P, Ti and Eu (0.46–2.63 ppm) contents in syenitic rocks make evident the chemical heterogeneity of them. The Eu/Eu* vs Ba/La diagram (Fig. 5) shows one magmatic group, whereas the syenite samples tend to be more enriched in Ba/La and Eu/Eu*.

6. Geochronology

AAC rocks intrude gabbros, metagranites and orthogneiss from the Paleo and Mesoproterozoic basement. In an attempt to define the basement crystallization age, two samples were selected for zircon U-Th-Pb geochronological studies. The first one is a metasyenogranite with protomylonitic texture (RRTJ-05), and the second is a metamorphosed alkali feldspar granite with mylonitic texture (RRTJ-07), both of them from the Rio Urubu Metamorphic Suite. From the AAC, a single sample from a nepheline syenite pluton (RRTJ-21) was dated using the zircon and baddeleyite U-Th-Pb methods. All the results are summarized in Table 2 and Table 3.

From sample RRTJ-05, 41 single zircon crystals were analyzed, 14 of them which presented 90% concordance. The crystals were slightly rounded, bipyramidal, with 180–300 μm in length, and length-to-width ratio varying from 1:5 to 2:3. They were usually colorless and transparent, although some grains were reddish to brownish. CL images showed sector zoning and incipient oscillatory zoning and rare dissolution/precipitation features (Fig. 6A). The U-Pb concordant age of 1931 ± 4 Ma (MSWD = 2.5) is interpreted as the crystallization age (Fig. 7A). An isolated zircon (Z146) yielded and age of 1896 Ma, probably resultant from Pb loss.

Eleven zircon grains from sample RRTJ-07 were analyzed, with 9 of them plotted on a Discordia. Most of the grains were reddish and/or brownish in colour, with overall 600 μm in length, andlength-to-width ratios of 1:3. CL images reveal a well-defined oscillatory zoning (Fig. 6B) with a brighter luminescent core, where dissolution and re-precipitation features are common. The Concordia Diagram from Fig. 7B suggests a crystallization age of 1958 ± 7 Ma, defined by the upper intercept in the Discordia plot. A single zircon grain (Z1)

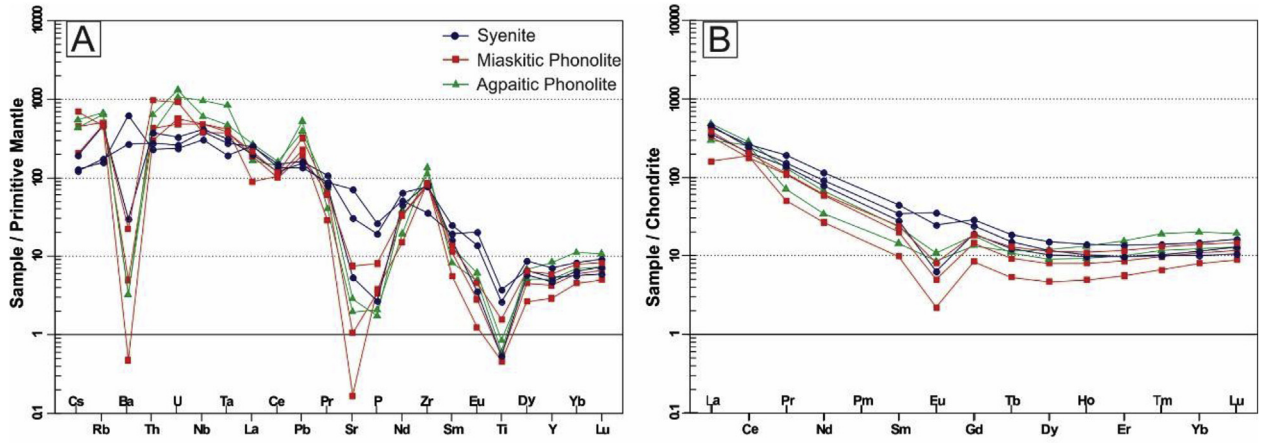

Fig. 4. Incompatible element signatures of the phonolites and syenites from AAC. A) Trace-element data normalized to primitive mantle (according to McDonough and Sun, 1995). B) Condrite normalized REE pattern (Boynton, 1984).

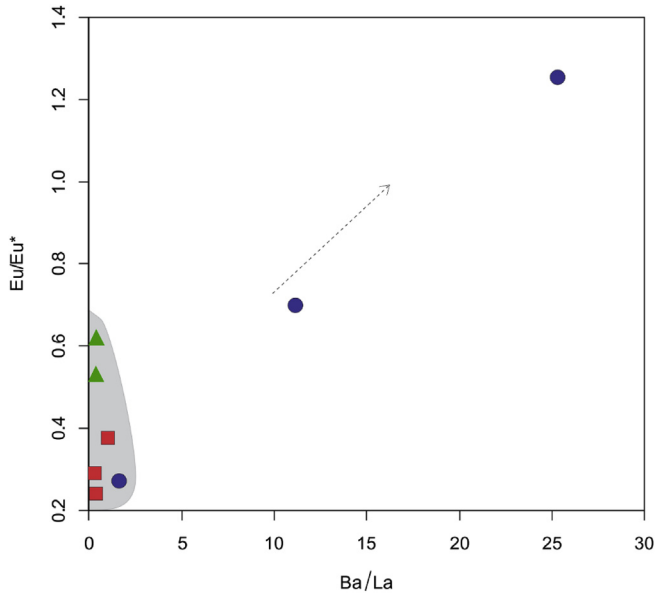

Fig. 5. Eu/Eu* vs Ba/La diagram for the alkaline rocks from AAC. The grey field represents the magmatic group of AAC. Possible trend of crustal contribution is indicated by the dashed arrow. Same symbols as for Fig. 3.

presented an age of 808 Ma, which was interpreted as resultant from Pb loss.

The age of the alkaline magmatism was obtained by applying the zircon U-Th-Pb method to the nepheline syenite (RRTJ-21). Twenty one zircon grains, separated in two families, were analyzed:

i) The first family plotted in the upper intercept, yielded an age around 1932 Ma, despite the slight Pb loss. All zircon grains were transparent, with a pale pink tint and preserved prismatic faces, except for a single rounded grain. The length of their main axes varied between 80 and 130 μm and the length-to-width ratio between 1:2 and 1:3. The CL images revealed just irregular igneous zoning, without overgrowing rims (Fig. 8).
ii) The second zircon family, composed of transparent, colorless to pale yellow grains, plotted in the lower intercept. They vary in shape from long and thin (1:3 to 1:5) prismatic crystals to rounded and wide (2:3 in ratio) and 80 and 250 μm long. Generally, the grains present inclusions and fractures, some being just small fragments. CL images revealed irregular and diffuse zoning, occasionally with incipient oscillatory zoning.

The results define two intercepts in the Concordia diagram (Fig. 9). The upper intercept at 1932 ± 14 Ma coincide with the crystallization age of the Rio Urubu Metamorphic Suite, b in which the alkaline syenite is hosted. The lower intercept at 111 ± 1 Ma (MSWD = 2.5), defined by eight zircon grains, is here assumed to be crystallization age of the alkaline magma. The Concordia diagram here obtained constitutes a classical example of assimilation of the older crustal material.

Besides zircon, it was also possible to separate baddeleyite from the alkaline syenite. This mineral is ideal for geochronology as it has high U contents and low common Pb. On top of that, baddeleyite is also resistant to Pb loss and rarely occurs as xenocrysts (Heaman and LeCheminant, 1993). Such characteristics provide precise ages with low associated errors, thus constituting an important method of dating magmatic events (Rubatto and Scambelluri, 2003; Heaman, 2009). $^{206}Pb/^{238}U$ ages were calculated using the FC-4b baddeleyite reference material (Paces and Miller, 1993). Phalaborwa (Heaman, 2009) and Sorkka (Söderlund et al., 2004) were analyzed as secondary reference materials.

The analyses were performed in 12 baddeleyite crystals; six of which were > 90% concordant. Baddeleyite crystals were euhedral and subhedral, with needle to tabular habits and reddish brown colour; occasionally their cleavage was pronounced. According to the results (Table 3) high values of U and Pb were obtained, differently from those obtained for zircons, which led to more concordant ages. The variation in $^{206}Pb/^{238}U$ ages up to 12% is attributed to ion emission according to some crystallographic orientations (Wingate and Compston, 2000).

Results provided a concordant age of 116 ± 3 Ma (MSWD = 1.7) (Fig. 10), interpreted as the crystallization age of the rock. This age is consistent with the ones obtained for zircons from the same sample, 111 ± 1 Ma (MSWD = 2.5). Even considering the variations in $^{206}Pb/^{238}U$, the baddeleyite results are attested and the age of the internal standard Phalaborwa was reproduced.

7. Petrogenetic considerations

The highly differentiated grades of the rocks from the AAC are marked by low contents of CaO, MgO, Fe_2O_3 and compatible trace elements, such as Co, Ni and Cr, as well as by high contents of incompatible trace elements. The negative anomalies of Ba, Sr, Eu, and P are related to the fractionation of biotite (Ba), plagioclase (Ba, Sr, Eu) and apatite (P). Besides that, the low contents of compatible elements suggests the fractionation of olivine, clinopyroxene and magnetite (MacDonald et al., 1995, 2008; Padilla and Gualda, 2016).

Petrographic variations in the syenites are represented by the relative scarcity of mafic minerals and the abundance of mesoperthitic orthoclase. The range of TiO_2, MgO and CaO contents in nepheline-

Table 2
Results of U-Pb isotope dating of zircon (LA-ICP-MS) from alkaline rock from AAC and its host rocks.

Zircon	*f*206 (%)	U (mg.g-1)	Th (mg.g-1)	Pb (mg.g-1)	Th/U calculated	$^{206}Pb/^{204}Pb$	$^{207}Pb/^{235}U$	1σ %	$^{206}Pb/^{238}U$	1σ %	Rho	$^{207}Pb/^{206}Pb$ (Age Ma)	2σ	$^{206}Pb/^{238}U$ (Age Ma)	2σ	207Pb/235U (Age Ma)	2σ	% conc[2]
Sample RRTJ-21: Nepheline-bearing syenite																		
Z12	0.09	2950	7190	305	2.44	19750	0.122	3.2	0.0179	2.4	0.75	333	31	114	3	117	4	34
Z13	0.29	900	1855	81	2.06	6465	0.120	3.3	0.0173	2.1	0.62	525	37	110	2	115	4	21
Z15	1.15	237	56	3	0.24	1625	0.110	6.9	0.0174	3.5	0.50	968	82	111	4	104	7	11
Z25	0.79	329	297	15	0.90	2380	0.120	4.0	0.0179	2.1	0.51	775	43	115	2	113	4	15
Z27	0.35	833	479	21	0.58	5380	0.113	3.3	0.0172	2.0	0.60	498	35	110	2	109	3	22
Z38	0.99	295	1039	43	3.53	1890	0.121	5.5	0.0169	2.7	0.49	899	58	108	3	112	6	12
Z45	0.80	396	808	35	2.04	2325	0.113	5.4	0.0172	2.7	0.50	760	53	110	3	106	6	14
Z47	0.23	1386	1642	70	1.18	8085	0.115	2.7	0.0174	1.7	0.62	467	33	111	2	110	3	24
Z14	2.95	87	778	36	8.94	634	0.151	8.6	0.0180	4.4	0.51	1540	100	115	5	125	11	7
Z17	0.92	276	631	30	2.29	2025	0.142	4.9	0.0176	2.7	0.54	1127	62	112	3	131	6	10
Z21	0.10	147	61	46	0.41	19450	5412	1.4	0.3343	1.3	0.96	1933	14	1856	21	1888	11	96
Z23	0.04	547	165	83	0.30	43150	3844	2.3	0.2370	2.2	0.96	1913	12	1366	27	1585	19	71
Z24	0.45	645	387	25	0.60	4160	0.167	4.7	0.0177	3.0	0.64	1028	64	113	3	157	7	11
Z26	0.62	326	10	1	0.03	3030	0.173	10.4	0.0275	5.1	0.49	700	120	175	9	162	16	25
Z29	1.80	163	197	13	1.21	1040	0.112	10.7	0.0179	4.6	0.43	1125	91	114	5	96	10	10
Z31	0.04	385	186	117	0.48	46700	5409	1.5	0.3295	1.5	0.98	1940	15	1831	24	1880	13	94
Z34	0.07	244	107	86	0.44	28450	5094	1.4	0.3132	1.5	1.06	1931	14	1752	23	1830	12	91
Z35	0.37	839	774	37	0.92	5090	0.109	4.6	0.0175	2.5	0.55	497	51	112	3	104	5	22
Z36	0.87	326	521	31	1.60	2155	0.139	5.0	0.0183	2.8	0.57	1062	57	116	3	130	6	11
Z44	0.69	459	1840	58	4.01	2710	0.130	10.8	0.0180	3.1	0.29	726	46	115	4	109	7	16
Z46	0.06	295	177	139	0.60	33800	5845	1.2	0.3553	1.1	0.95	1934	12	1961	19	1952	10	101
Sample RRTJ-05: Metasyenogranite																		
Z122	0.08	243	81	62	0.33	22650	5736	1.3	0.3433	1.4	1.03	1883	14	1899	22	1936	11	101
Z124	0.09	227	149	122	0.66	20900	5689	1.3	0.3459	1.4	1.07	1861	16	1912	23	1930	11	103
Z126	0.11	183	107	88	0.58	16750	5710	1.5	0.3445	1.6	1.03	1884	16	1911	25	1930	13	101
Z127	0.07	317	189	141	0.59	26850	5648	1.6	0.3440	1.5	0.99	1897	17	1904	25	1925	13	100
Z128	0.05	420	176	136	0.42	34200	5590	1.8	0.3448	1.9	1.05	1886	18	1907	31	1910	15	101
Z129	0.07	353	178	136	0.50	28150	5520	2.0	0.3442	1.9	0.93	1891	20	1905	30	1903	17	101
Z130	0.06	431	267	220	0.62	33900	5754	1.6	0.3500	1.6	1.02	1875	16	1931	27	1933	14	103
Z131	0.07	347	183	149	0.53	27300	5795	1.6	0.3512	1.7	1.09	1885	19	1940	28	1943	14	103
Z134	0.06	434	217	191	0.50	31800	5753	1.7	0.3503	1.9	1.08	1867	18	1935	30	1939	15	104
Z136	0.12	229	112	96	0.49	16200	5716	1.7	0.3496	1.7	1.03	1864	20	1929	29	1929	15	103
Z140	0.24	114	54	48	0.47	7820	5660	2.8	0.3456	2.5	0.88	1856	27	1918	41	1920	24	103
Z146	0.18	151	98	86	0.65	10145	5510	2.2	0.3422	2.1	0.98	1784	23	1897	35	1896	19	106
Z156	0.18	158	65	61	0.41	10660	5761	1.7	0.3500	1.7	1.00	1845	19	1928	28	1932	15	104
Z158	0.23	122	60	57	0.49	8285	5840	2.1	0.3536	1.9	0.92	1856	20	1943	32	1945	17	105
Sample RRTJ-07: Meta alcali feldspar granite																		
Z1	0.03	859	900	260	1.05	55300	2114	1.8	0.1338	1.9	1.11	1867	11	808	15	1156	12	43
Z2	0.02	615	314	257	0.51	98800	5579	1.2	0.3384	1.3	1.09	1933	11	1877	21	1911	10	97
Z3	0.02	530	335	278	0.63	82500	5899	1.2	0.3619	1.2	1.04	1935	12	1987	21	1958	10	103
Z4	0.04	316	212	172	0.67	50400	5353	1.4	0.3254	1.4	1.00	1924	11	1814	22	1871	12	94
Z5	0.04	318	159	130	0.50	48900	6000	1.7	0.3530	1.4	0.85	1966	18	1946	24	1953	13	99
Z6	2.71	786	569	245	0.72	691	3230	3.1	0.1840	3.7	1.19	2096	17	1078	37	1432	24	51
Z7	0.07	165	59	73	0.36	25500	6060	1.8	0.3269	2.1	1.18	2159	17	1819	34	1984	15	84
Z8	0.04	349	163	132	0.47	52350	5748	1.2	0.3518	1.2	1.05	1925	12	1941	20	1934	10	101
Z9	0.04	277	144	121	0.52	42050	5814	1.2	0.3592	1.3	1.07	1930	13	1977	22	1943	10	102

Table 3
Results of U-Pb isotope dating of baddeleyite (LA-ICP-MS) of the AAC nepheline-bearing syenite. ND = not determined.

Baddeleyite	*f*206 (%)	U (mg.g-1)	Th (mg.g-1)	Pb (mg.g-1)	Th/U calculated	$^{206}Pb/^{204}Pb$	$^{207}Pb/^{235}U$	1σ %	$^{206}Pb/^{238}U$	1σ %	Rho	$^{207}Pb/^{206}Pb$	2σ Age Ma)	$^{206}Pb/^{238}U$	2σ (Age Ma)	$^{207}Pb/^{235}U$	2σ (Age Ma)	% conc[2]
Sample RRTJ-21: Nepheline-bearing syenite																		
Bd1	−9.12	296	ND	80	ND	−205	0.119	18.5	0.01842	5.2	0.28	115	20	117.6	6	40	290	102
Bd3	0.40	8.25E+04	ND	1.80E+05	ND	4643	0.1236	6.4	0.0181	7.2	1.12	118.3	7	115.7	8	175	91	98
Bd4	1.11	3.60E+04	ND	7.70E+04	ND	1688	0.123	20.3	0.0179	17.9	0.88	117	22	114	20	490	210	97
Bd6	0.26	8.43E+04	ND	2.71E+05	ND	7333	0.136	16.9	0.019	17.4	1.03	130	20	121	21	300	200	93
Bd10	0.07	1.40E+05	ND	1.63E+05	ND	27444	0.1182	5.0	0.01713	5.6	1.12	113.5	5	109.5	6	310	120	96
Bd12	0.32	1.33E+05	ND	1.97E+05	ND	5783	0.1237	5.7	0.01801	4.8	0.84	118.4	6	115.1	5	219	61	97

bearing syenites and nepheline-bearing alkali feldspar syenite is related to mafic minerals, essentially biotite and amphibole. Eu anomalies are related to plagioclase fractionation as observed in the petrography. The smooth positive Eu anomaly in one (in Fig. 4) syenite sample is due the presence of plagioclase cumulate. The marked decrease in Ba in more alkaline varieties indicates that in these rocks this element has been retained by plagioclase (Hanson, 1978; Padilla and Gualda, 2016).

The nepheline-bearing syenite has a metaluminous character, with an alkalinity index between transitional to peralkaline. In spite of the decrease in alkalis, there is a increase in alumina content. The fractional crystallization of feldspar tends to enrich the melt in sodium while depleting it in alumina, from metaluminous to peralkaline with increasing differentiation (Frost and Frost, 2008). However, there is a decrease in alkalinity in the magmatic chamber, also evidenced by the substitution of arfvedsonite by calcic amphibole.

The phonolites are the most evolved lithotypes identified in the AAC. According to the alkalinity index, these rocks are divided in peralkaline and metaluminous with peralkaline tendency. The most peralkaline specimen can be classified as agpaitic because of the presence of eudialyte (Le Maitre, 2002). The others are classified as miaskitic (Sørensen, 1974, 1992, 1997).

The agpaitic phonolites represent the most evolved rocks of the undersaturate alkaline magmatism. Notably, Na_2O contents in these phonolites are the highest, which is probably due to the abundance of phenocrysts and nepheline in the groundmass, whereas the miaskitic phonolites commonly present sanidine phenocrysts. The formation of magmatic eudialyte requires a certain level of NaCl activity in the melt (Marks et al., 2011); besides, the presence of sodalite is a good indicator of a high-temperature silicate magma enriched in NaCl (Sharp et al., 1989). The presence of cryolite (Na_3AlF_6) in the agpaitic rocks suggests the interaction with sodic and fluoride-rich fluids. The presence of eudialyte and marked alkali and HFSE enrichment represent the residual agpaitic magma in which the phonolites were generated.

Petrographic and geochemical data suggest fractional crystallization as the main formation process for the AAC. Marsh (2010) shows that world-wide phonolites have broadly similar trace element patterns, which reflects the pronounced role for fractional crystallization in their petrogenesis. The rocks from the AAC are characterized by relatively high incompatible element contents and high LREE/HREE ratios. The phonolites and syenites share some important characteristics such as enrichment of incompatible elements and similar trace element patterns, which indicate that they have been generated by similar fractionation processes involving closely related parental melts.

Although the similarities in incompatible patterns, there are some differences in their intensities. The phonolites show intense negative anomalies of Ba, Sr, P and Ti compared to syenites. Furthermore, one syenite sample has much higher Ba, Sr and Eu contents than all other rocks from AAC. Ba, Sr and Eu are compatible elements in plagioclase structure (Padilla and Gualda, 2016). Most of these rocks have almost similar Eu/Eu* vs Ba/La ratios. Fig. 5 shows a progressive increase of these ratios in syenites, which is probably due to accumulation and/or resorption of plagioclase. The variable trace elements enrichments in syenites could be related to the country rock assimilation. Ba is also high compatible in biotite structure (Tischendorf et al., 2001), but the low contents of Rb suggests that biotite doesn't play an important role in these process.

A miaskitic phonolite (RRTJ-30B) presents an anomalous enrichment in MgO and in compatible elements, such as Cr, Ni and Co. Petrographically, the sample presents xenocrysts of olivine and pyroxene that were incorporated from an olivine gabbro from the host basement. Assimilation of older crustal material is indicated by the presence of inherited Proterozoic zircons in the nepheline-bearing syenite pluton and xenocrysts in phonolite; however, it was not significant during the formation of the alkaline rocks.

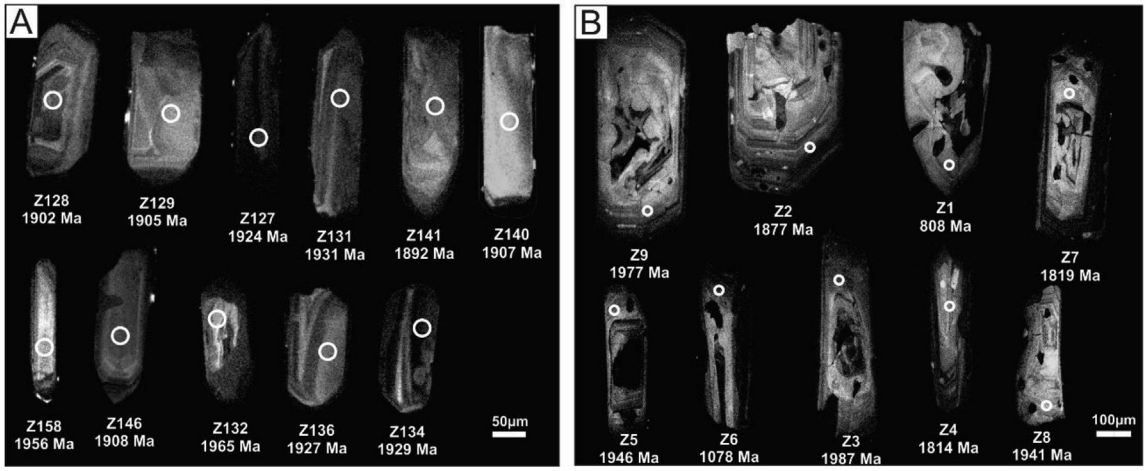

Fig. 6. CL images of zircon grains from the Rio Urubu Metamorphic Suite, samples RRTJ-05 (A) and RRTJ-07 (B). Note the circle indicating the spot position.

8. Implications for the regional tectonic evolution

The precise U-Pb zircon/baddeleyite crystallization ages of 111 ± 1 Ma and 116 ± 3 Ma indicates that this period of alkaline magmatism corresponds to the opening of the Equatorial Atlantic Ocean and is related to a structural reactivation of weak zones in the Amazonian Craton. The opening of the Equatorial Atlantic Ocean occurred during the Aptian-Albian boundary, contemporaneous with the onset of seafloor spreading in the Central Atlantic. The separation of the continental-oceanic boundary in the Equatorial Atlantic took place around 100 Myr ago, the time of the final breakup (Moulin et al., 2010; Granot and Dyment, 2015). Furthermore, Bonatti (1996) assumes that an anomalously low temperature of the equatorial upper mantle existed in the Cretaceous at the time of the opening of the Equatorial Atlantic rift, and this would imply a pre-opening equatorial continental lithosphere colder and thicker than normal.

Matton and Jébrak (2009) demonstrate that the mid-Cretaceous (125-80 Ma) was characterized by abnormal alkaline activity in the peri-Atlantic continental margins, which is associated with two major plate reorganizations, and that intrusions were associated with the reactivation of pre-existing structures. According to Bonatti (1996), the Mesozoic reactivation in the Amazonian Craton could be related to wrenching of the thick, cold equatorial lithosphere, due to the attempted equatorial propagation of the proto-Atlantic rifts from north and south.

The Central Guyana Domain, a portion of the Guyana Shield that encompasses the AAC rocks, has a complex structure dominated by important transcurrent shear zones. Its geodynamic evolution occurred during the Paleo and Mesoproterozoic related to three important tectonic-thermal events: (i) post-Transamazonian; (ii) Itã, and (iii) K'Mudku (Gaudette et al., 1996; CPRM, 1999; Fraga, 2002; Reis et al., 2003; Santos et al., 2000, 2006b; Almeida, 2006; Almeida et al., 2008). The majority of the structures associated with alkaline complexes are older weakness zones that were repeatedly reactivated during post tectono-thermal events (Pirajno, 2015). Even so, weakness zones could be intensified during rifting, reaching depths that allowed them to serve as conducts for alkaline magma (Fig. 11).

In this extensional context the reactivation of ancient zones of lithospheric structural weakness is favoured, particularly the Proterozoic shear zones. Indications in this sense are given by the alignment of the alkaline occurrences following major faults. Intraplate extension led to the development of the Tacutu basin, settled from Triassic faults/fractures reactivations (period of the first evidence of tholeiitic magmatism of the CAMP in the form of dykes). In this way, the rise of alkaline and tholeiitic magma is related to the decompression of the source area due to lithospheric thinning during the opening of Equatorial Atlantic Ocean.

AAC is the youngest alkaline complex in the Guyana Shield and this

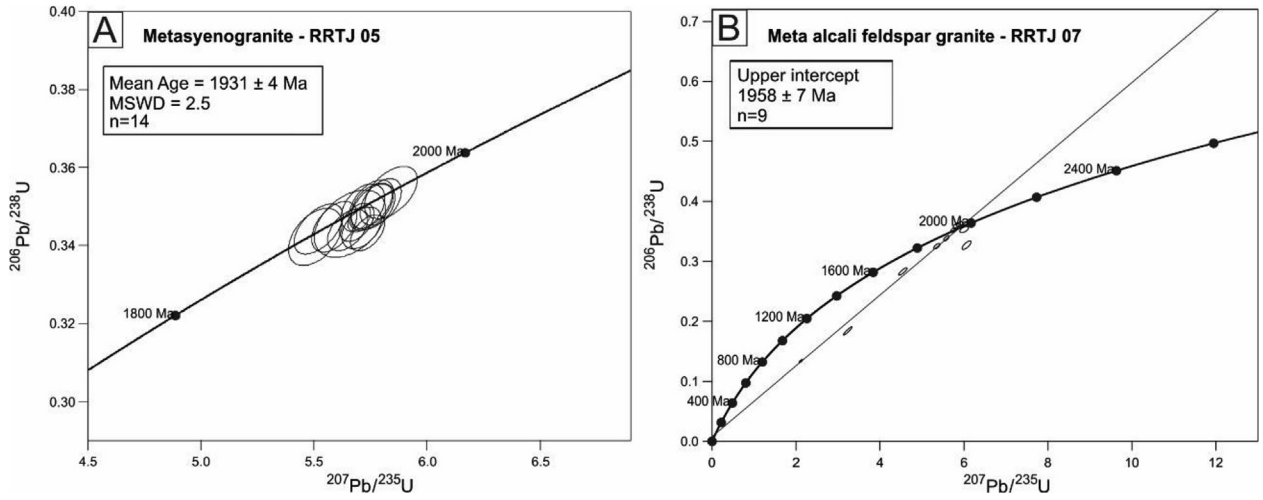

Fig. 7. Zircon U-Pb crystallization ages of the orthoderived basement (Rio Urubu Metamorphic Suite). A) The Concordia Diagram for metasyenogranite with protomylonitic texture (RRTJ-05) with concordia age defined by 14 grains. B) Diagram for a metamorphosed alkali feldspar granite with mylonitic texture (RRTJ-07), in which 9 grains define a Discordia.

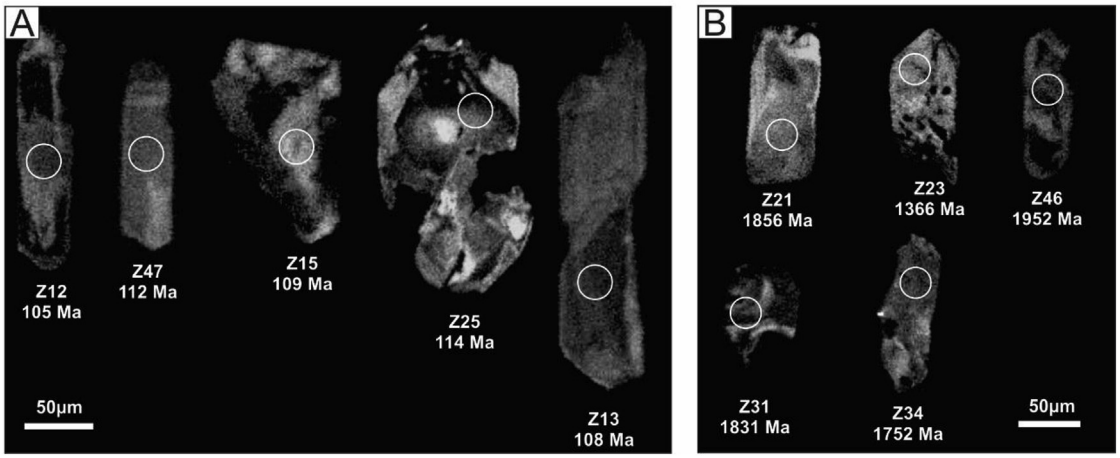

Fig. 8. CL images of (A) zircon grains from the alkaline rocks and (B) zircon grains inherited from the basement.

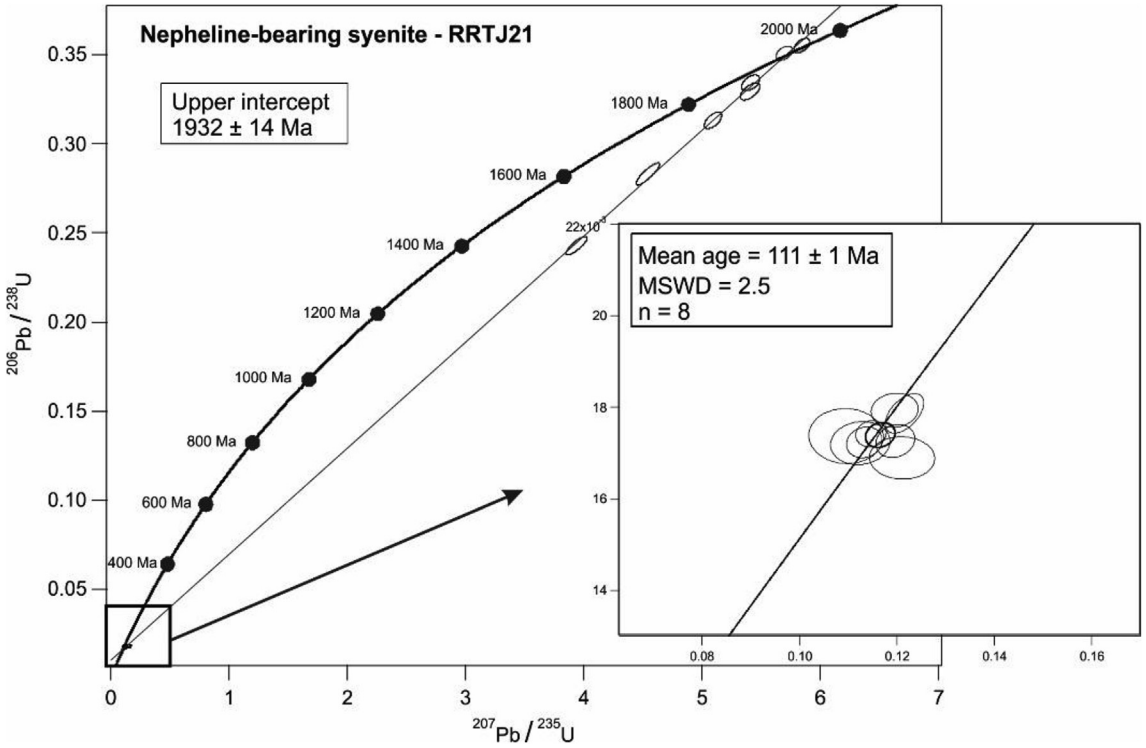

Fig. 9. Concordia diagram for nepheline-bearing syenite (RRTJ-21), highlighting the lower intercept defined by eight zircon grains. The zircon grains from the basement display incipient Pb loss at the upper intercept.

magmatic activity corresponds to the same period of the Tacutu basin filling (Eiras and Kinoshita, 1988, 1990; Vaz et al., 2007), evidencing a period of relative tectonic stability and suggesting that the progressive subsidence contributed to structural reactivation in deep crustal levels. During this interval, lithospheric thinning, which was responsible for the high rates of mantle melting, ceased.

The ages of the alkaline pluton and of the basaltic manifestations suggest an extensive magmatism related to rifting. The most expressive occurred during the extension phase, typically along the rift margins where basaltic manifestations are observed. The tholeiitic magmatism comprises the formation of dykes of the CAMP around 200 Ma and flooding between 153 and 135 Ma (Marzoli et al., 1999; Leal et al., 2000; Reis et al., 2004, 2006). In this context, with the progressive lithospheric thinning, basaltic and andesitic flooding occurred between the Upper Jurassic and the Lower Cretaceous, with a gap of 50 Ma since the first occurrences of mafic dykes in the Upper Triassic. The extensional phase responsible for the opening of grabens in South America probably started in the Lower Triassic and continued along the Jurassic. The Meso- and Neo-Jurassic volcanic rocks are representative of the culminating event of this extensional phase (Gust et al., 1985).

The orthoderived basement of essentially granitic composition (Rio Urubu Metamorphic Suite) hosts the alkaline rocks and present U-Pb zircon ages of 1931 ± 4 Ma and 1958 ± 7 Ma. The presence of zircon xenocrysts in the AAC nepheline-bearing syenite pluton indicates that the alkaline magma was contaminated with Paleoproterozoic crustal rocks. According to Markl et al. (2001), strongly Si-undersaturated melts are highly reactive with granitic wall rocks.

9. Conclusion

The rocks of AAC have metaluminous to peralkaline character, potassic to sodic affinity and miaskitic to agpaitic mineral compositions.

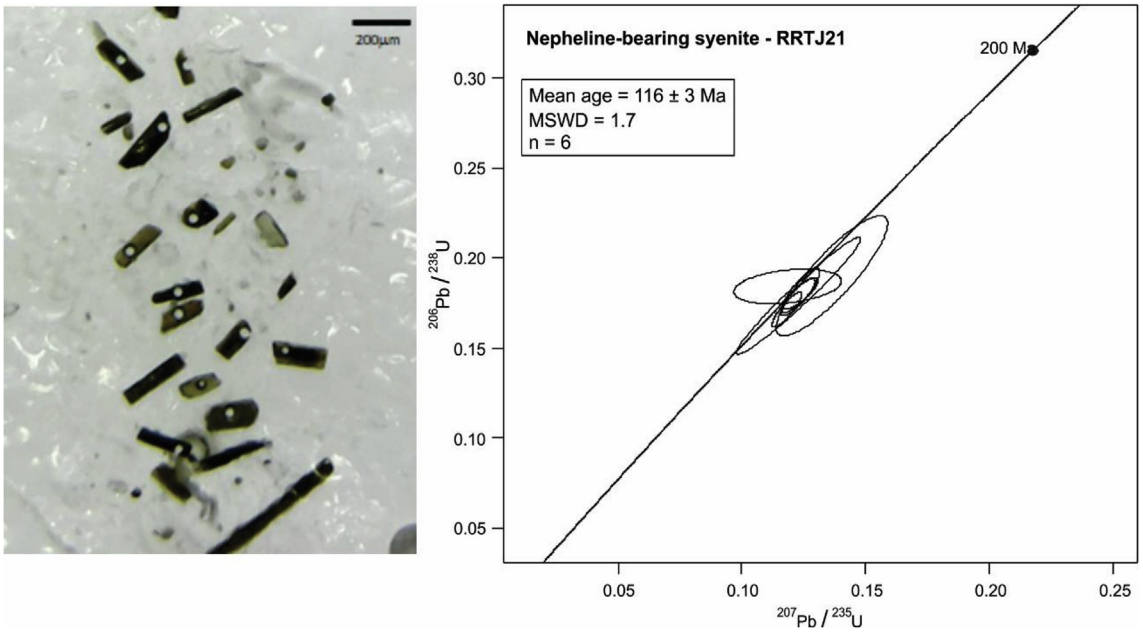

Fig. 10. Picture of the baddeleyites analyzed and U-Pb isotope diagram showing a concordia curve for baddeleyite from nepheline-bearing syenite RRTJ-21, yielding a concordant age of 116 ± 3 Ma.

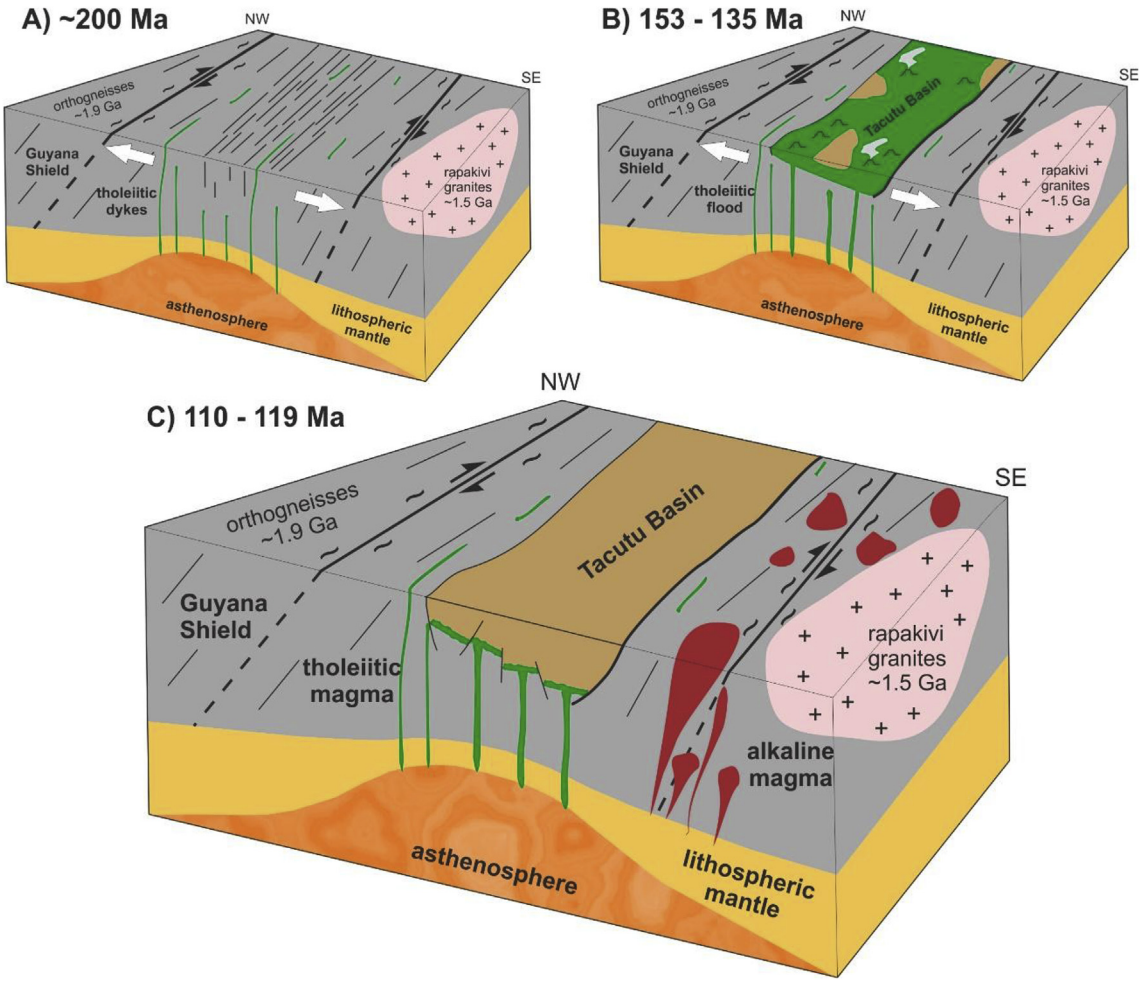

Fig. 11. Schematic block showing major weakness zones in Guyana Shield which were reactivated during the break-up of Gondwana, generating magmatism and intracontinental rifting. The initial rift phase of the Tacutu Basin is marked by tholeiitic magmatism represented by dykes of the CAMP; ca. 200 Ma (inset A) and volcanic floods between 153 and 135 Ma (inset B). Generation of alkaline magmatism between 110 and 119 Ma (considering age error brackets) and the emplacement clearly controlled by a tectonic extensional regime, in which the spatial disposition of the alkaline rocks following important Precambrian shear zones (C).

The agpaitic phonolites represent the most differentiated rocks, a residual magma enriched in sodic and fluoride-bearing fluids. The phonolites and syenites share important geochemical characteristics, which suggest that they are comagmatic. The trace element patterns are characterized by negative anomalies of Eu, Ba, Sr, P and Ti and strong LREE fractionation. Despite the similarities in incompatible patterns, there are some differences in the syenites behaviour. Petrography shows alkaline amphibole substitution by more calcic amphibole and the presence of xenocrysts. In addition to the geochemical and petrographic data, there are inherited zircons of Precambrian age in nepheline-bearing syenite, indicate which crustal assimilation occurred.

The U-Pb ages of 111 ± 1 Ma and 116 ± 3 Ma obtained for the nepheline-bearing syenite suggest a relationship between the Lower Cretaceous magmatism and the opening of Equatorial Atlantic Ocean. The emplacement of the Apiaú Alkaline Complex was clearly controlled by a tectonic extensional regime, in which the spatial disposition of the alkaline rocks following major faults of the Guyana Shield indicates a structurally controlled emplacement history. Crystallization ages correspond to the period of filling of the Tacutu Basin and suggest relative stable tectonic conditions necessary to generate small degrees of partial melting, as well as progressive subsidence contributing to the reactivation of major structures. Zircon U-Pb crystallization ages of 1931 ± 4 Ma and 1958 ± 7 Ma were obtained for the orthoderived basement of granitic composition which hosts the alkaline rocks.

Acknowledgements

We thank the Brazilian agency CAPES/PROEX for the financial support and the fellowship granted to the first author. We are very grateful to the SGM mining company, especially Marcelo Almeida, Claumilde Vasconcelos and Paulo Orcioli for their valuable assistance during fieldwork. Special thanks to Dr. V. Pease and Dr. C. Wohlgemuth-Ueberwasser, from the University of Stockholm, for the support gave to baddeleyite dating. We also would like to thank to the reviewers, Dr. Angelo De Min and an anonymous one, for their constructive comments that certainly improved the manuscript considerably. This manuscript was significantly improved by the constructive comments of Prof. Rogério Azzone, which are greatly appreciated.

References

Almeida, F.F.M., 1986. Distribuição regional e relações tectônicas do magmatismo pós-paleozóico no Brasil. Rev. Bras. Geociencias 16, 325–349.
Almeida, M.E., 2006. Evolução geológica da porção centro-sul do Escudo das Guianas com base no estudo Geoquímico, Geocronológico e Isotópico dos granitoides paleoproterozóicos do sudeste de Roraima, Brasil. PhD thesis. Federal University of Pará, pp. 227.
Almeida, M.E., Macambira, M.J.B., Valente, S. de C., 2008. New geological and single-zircon Pb evaporation data from the Central Guyana Domain, southeastern Roraima, Brazil: tectonic implications for the central region of the Guyana Shield. J. S. Am. Earth Sci. 26, 318–328.
Bailey, D.K., 1977. Lithosphere control of continental rift magmatism. J. Geol. Soc. 133, 103–106.
Begg, G.C., Griffin, W.L., Natapov, L.M., O'Reilly, S.Y., Grand, S.P., O'Neill, C.J., Hronsky, J.M.A., Djomani, Y.P., Swain, C.J., Deen, T., Bowden, P., 2009. The lithospheric architecture of Africa: seismic tomography, mantle petrology, and tectonic evolution. Geosphere 5, 23–50.
Biondi, J.C., 2005. Brazilian mineral deposits associated with alkaline and alkaline carbonatite complexes. In: Comin-Chiaramonti, P., Gomes, C.B. (Eds.), Mesozoic to Cenozoic Alkaline Magmatism in the Brazilian Platform. Edusp/Fapesp, São Paulo, pp. 707–750.
Bonatti, E., 1996. Equatorial mantle thermal minimum. Earth Planet Sci. Lett. 143, 147–160.
Borges, F.R., 1990. Projeto Serra Do Repartimento. Technical Report. CPRM 30 pp.
Boynton, W.V., 1984. Cosmochemistry of the rare Earth elements: meteorite studies. In: Henderson, P. (Ed.), Rare Earth Element Geochemistry: Developments in Geochemistry 2. Elsevier, Amsterdam, pp. 63–114.
Brandão, R.L., Freitas, A.F.F., 1994. Serra Do Ajarani: Folha NA.20-X- C- VI. Technical Report. CPRM, pp. 153.
Cordani, U.G., Fraga, L.M., Tassinari, C.C.G., Brito-Neves, B.B., 2010. On the origin and tectonic significance of the intra-plate events of Grenvillian-type age in South America: a discussion. J. S. Am. Earth Sci. 29, 143–159.
Costa, J.B.S., Pinheiro, R.V.L., Reis, N.J., Pessoa, M.R., Pinheiro, S.S., 1991. O hemi-graben do Tacutu: uma estrutura controlada pela geometria do Cinturão de Cisalhamento Guiana Central. Geociencias 10, 119–130.
Costa, S.S., 2005. Delimitação do arcabouço tectônico do Cinturão Guiana Central, estado de Roraima, com base na análise integrada dos dados geofísicos, geológicos, isotópicos e imagens de satélite. PhD thesis. University of Campinas, pp. 189.
Cotta, A.J.B., Enzweiler, J., 2011. Classical and new procedures of whole rock dissolution for Trace Element determination by ICP-MS. Geostand. Geoanal. Res. 1–24.
CPRM, Companhia de Pesquisa de Recursos Minerais, 1999. Programa Levantamentos Geológicos Básicos do Brasil. Roraima Central, Folhas NA.20-X-B e NA.20-X-D (integrais), NA.20-X-A, NA.20-X-C, NA.21-V-A e NA.21-V-C (parciais). Escala 1:500.000. Technical report. CPRM, pp. 166.
Eiras, J.F., Kinoshita, E.M., 1988. Evidências de movimentos transcorrentes na Bacia do Tacutu. Bol. Geociencias Petrobras 2, 193–208.
Eiras, J.F., Kinoshita, E.M., 1990. Geologia e perspectivas petrolíferas da Bacia do Tacutu. In: Gabaglia, G.P.R., Milani, E.J. (Eds.), Origem e Evolução de Bacias Sedimentares. Petrobras, Rio de Janeiro, pp. 197–220.
Fitton, J.G., Upton, B.G.J., 1987. Alkaline Igneous Rocks. Geological Society of London, London, pp. 568.
Figueiredo, R.F., 2016. Contexto tectônico do Complexo Alcalino Apiaú– Roraima: Aerogeofísica, petrologia e geocronologia U-Pb. M.S. thesis, University of Campinas 102 pp.
Fraga, L.M.B., Almeida, M.E., Macambira, M.J.B., 1997. First lead-lead zircon ages of charnockitic rocks from Central Guiana Belt (CGB) in the state of Roraima, Brazil. In: South-american Symposium on Isotope Geology. Campos do Jordão, SP, pp. 115–117.
Fraga, L.M.B., 2002. A associação anortosito-mangerito-granito rapakivi (AMG) do Cinturão Guiana Central, Roraima, e suas encaixantes paleoproterozóicas: evolução estrutural, geocronologia e petrologia. PhD thesis. Federal University of Pará, pp. 351.
Fraga, L.M., Dall'Agnol, R., Costa, J.B.S., Macambira, M.J.B., 2009. The mesoproterozoic mucajaí anorthosite-mangerite-rapakivi granite complex, amazonian craton, Brazil. Can. Mineral. 47, 1469–1492.
Frost, B.R., Frost, C.D., 2008. A geochemical classification for feldspathic rocks. J. Petrol. 49, 1955–1969.
Gaudette, H.E., Olszewski Jr., W.J., Santos, J.O.S., 1996. Geochronology of precambrian rocks from the northern part of guiana shield, state of Roraima, Brazil. J. S. Am. Earth Sci. 9, 183–195.
Gibson, S.A., Thompson, R.N., Leonardos, O.H., Dickin, A.P., Mitchell, J.G., 1995. The Late Cretaceous impact of the Trindade mantle plume: evidence from large-volume, mafc potassic magmatism in SE Brazil. J. Petrol. 36, 189–229.
Gibson, S.A., Thompson, R.N., Leonardos, O.H., Dickin, A.P., Mitchell, J.G., 1999. The limited extent of plume-lithosphere interactions during continental flood-basalt genesis: geochemical evidence from Cretaceous magmatism in southern Brazil. Contrib. Mineral. Petrol. 137, 147–169.
Gomes, C.B., Ruberti, E., Morbidelli, L., 1990. Carbonatite complexes from Brazil: a review. J. S. Am. Earth Sci. 3, 51–63.
Gomes, C.B., Comin-Chiaramonti, P., 2005. An introduction to the alkaline and alkaline-carbonatitic magmatism in and around the Paraná Basin. In: Comin-Chiaramonti, P., Gomes, C.B. (Eds.), Mesozoic to Cenozoic Alkaline Magmatism in the Brazilian Platform. Edusp/Fapesp, São Paulo, pp. 21–29.
Granot, R., Dyment, J., 2015. The cretaceous opening of the south Atlantic Ocean. Earth Planet Sci. Lett. 414, 156–163.
Gust, D.A., Biddle, K.T., Phelps, D.W., Uliana, M.A., 1985. Associated middle to late Jurassic volcanism and extension in southern South America. Tectonophysics 116, 223–253.
Hanson, G.N., 1978. The application of trace elements to the petrogenesis of igneous rocks of granitic composition. Earth Planet Sci. Lett. 38, 26–43.
Heaman, L.M., LeCheminant, A.N., 1993. Paragenesis and U-Pb systematics of baddeleyite (ZrO2). Chem. Geol. 110, 95–126.
Heaman, L.M., 2009. The application of U–Pb geochronology to mafic, ultramafic and alkaline rocks: an evaluation of three mineral standards. Chem. Geol. 261, 43–52.
Heinonen, A.P., Fraga, L.M., Rämö, O.T., Dall'Agnol, R., Mänttäri, I., Andersen, T., 2012. Petrogenesis of the igneous Mucajaí AMG complex, northern Amazonian craton - geochemical, U-Pb geochronological, and Nd-Hf-O isotopic constraints. Lithos 151, 17–34.
Leal, A.B.M., Girardi, V.A.V., Leal, L.R.B., 2000. Petrologia e geoquímica do magmatismo básico mesozoico da Suíte Básica Apoteri, estado de Roraima. Geochim. Bras. 14, 155–174.
Le Maitre, R.W., 2002. Igneous Rocks: a Classification and Glossary of Terms. Cambridge University Press, New York, pp. 236.
MacDonald, R., Davies, G.R., Upton, B.G.J., Dunkley, P.N., Smith, M., Leat, P.T., 1995. Petrogenesis of silali volcano, gregory rift, Kenya. J. Geol. Soc. 152, 703–720.
MacDonald, R., Belkin, H.E., Fitton, J.G., Rogers, N.W., Nejbert, K., Tindle, A.G., Marshall, A.S., 2008. The roles of fractional crystallization, magma mixing, crystal mush remobilization and volatile-melt interactions in the genesis of a young basalt-peralkaline rhyolite Suite, the Greater Olkaria Volcanic Complex, Kenya Rift Valley. J. Petrol. 49, 1515–1547.
Marsh, J.S., 2010. The geochemistry and evolution of Palaeogene phonolites, central Namibia. Lithos 117, 149–160.
Markl, G., Marks, M.W., Schwinn, G., Sommer, H., 2001. Phase equilibrium constraints on intensive crystallization parameters of the Ilímaussaq Complex, South Greenland. J. Petrol. 42, 2231–2257.
Marks, M.A.W., Hettmann, K., Schilling, J., Frost, B.R., Markl, G., 2011. The mineralogical diversity of alkaline igneous rocks: critical factors for the transition from miaskitic to agpaitic phase assemblages. J. Petrol. 52, 439–455.
Marzoli, A., Renne, P.R., Piccirillo, E.M., Ernesto, M., Bellieni, G., De Min, A., 1999.

Extensive 200-million-year-old continental flood basalts of the central atlantic magmatic province. Science 284, 616–618.
Matton, G., Jébrak, M., 2009. The Cretaceous Peri-Atlantic Alkaline Pulse (PAAP): deep mantle plume origin or shallow lithospheric break-up? Tectonophysics 469, 1–12.
McDonough, W.F., Sun, S., 1995. The composition of the Earth. Chem. Geol. 120, 223–253.
Middlemost, E.A.K., 1975. The basalt clan. Earth Sci. Rev. 11, 337–364.
Montalvão, R.M.G., Muniz, M.C., Issler, R.S., Dall'Agnol, R., Lima, M.I.C., Fernandes, P.E.C.A., Silva, G.G., 1975. Projeto Radam Brasil 8v: Folha NA.20- Boa Vista e parte das folhas NA.21 - Tumucumaque, NB.20 – Roraima e NB.21. DNPM, Rio de Janeiro, pp. 403.
Moulin, M., Aslanian, D., Unternehr, P., 2010. A new starting point for the south and equatorial Atlantic Ocean. Earth Sci. Rev. 98, 1–37.
Morbidelli, L., Gomes, C.B., Beccaluva, L., Brotzu, P., Conte, A.M., Ruberti, E., Traversa, G., 1995. Mineralogical, petrological and geochemical aspects of alkaline and alkaline carbonatite associations from Brazil. Earth Sci. Rev. 39, 135–168.
Navarro, M.S., Tonetto, E.M., Oliveira, E.P., 2015. LA-SF-ICP-MS U-Pb zircon dating at university of Campinas, brazi. In: IAG, Geoanalysis 2015, (Leoben, CD-ROM).
Paces, J.B., Miller, J.D., 1993. Precise U–Pb ages of Duluth complex and related mafic intrusions, northeastern Minnesota: geochronological insights to physical, petrogenetic, paleomag- netic, and tectonomagmatic processes associated with the 1.1 Ga midcontinent Rift system. J. Geophys. Res. 98, 13997–14013.
Pagano, D.S., Galliski, M.Á., Márquez-Zavalía, M.F., Colombo, F., 2016. Petrology and mineralogy of the La peña igneous complex, mendoza, Argentina: an alkaline occurrence in the Miocene magmatism of the southern central andes. J. S. Am. Earth Sci. 67, 158–179.
Padilla, A.J., Gualda, G.A.R., 2016. Crystal-melt elemental partitioning in silicic magmatic systems: an example from the Peach Spring Tuff high-silica rhyolite, Southwest USA. Chem. Geol. 440, 326–344.
Pirajno, F., 2015. Intracontinental anorogenic alkaline magmatism and carbonatites, associated mineral systems and the mantle plume connection. Gondwana Res. 27, 1181–1216.
Reis, N.J., Fraga, L.M., Faria, M.S.G., Almeida, M.E., 2003. A geologia de Roraima. Geol. France 2–3–4, 121–134.
Reis, N.J., Faria, M.S.G., Almeida, M.E., Oliveira, M.A., 2004. Folhas NA.20-Boa Vista e NB.20-Roraima. In: Schobbenhaus, C., Gonçalves, J.H., Santos, J.O.S., Abram, M.B., Leão Neto, R., Matos, G.M.M., Vidotti, R.M., Ramos, M.A.B., Jesus, J.D.A.de (Eds.), Carta Geológica do Brasil ao Milionésimo, Sistema de Informações Geográficas-SIG, Programa Geologia do Brasil. CPRM, Brasília (CD-ROM).
Reis, N.J., Szatmari, P., Wanderley Filho, J.R., York, D., Evensen, N.M., Smith, P.E., 2006. Dois eventos de magmatismo máfico mesozóico na fronteira Brasil-Guiana, Escudo das Guianas: enfoque à região do rifte Tacutu-North Savannas. In: 43º Congresso Brasileiro de Geologia, Aracaju, 459–46.
Riccomini, C., Velázquez, V.F., Gomes, C.B., 2005. Tectonic controls of the mesozoic and cenozoic alkaline magmatism in central-southeastern brazilian platform. In: Comin-Chiaramonti, P., Gomes, C.B. (Eds.), Mesozoic to Cenozoic Alkaline Magmatism in the Brazilian Platform. Edusp/Fapesp, São Paulo, pp. 31–55.
Rubatto, D., Scambelluri, M., 2003. U–Pb dating of magmatic zircon and metamorphic baddeleyite in the Ligurianeclogites (Voltri Massif, Western Alps). Contrib. Mineral. Petrol. 146, 341–355.
Salas, N.J., Santos, J.O.S., 1974. Determinações geocronológicas pelo método da birrefringência em phonolite na área do Projeto Norte da Amazônia. In: 28º Congresso Brasileiro de Geologia, Porto Alegre, pp. 221–224.
Santos, J.O.S., Hartmann, L.A., Gaudette, H.E., Groves, D.I., Mcnaughton, N.J., Fletcher, I.R., 2000. A new understanding of the Provinces of the Amazon Craton based on integration of field mapping and U-Pb and Sm-Nd Geochronology. Gondwana Res. 3, 453–488.
Santos, J.O.S., Hartmann, L.A., Faria, M.S.G., Riker, S.R.L., Souza, M.M., Almeida, M.E., McNaughton, N.J., 2006a. A compartimentação do Cráton Amazonas em Províncias: avanços ocorridos no período 2000-2006. In: 9º Simpósio de Geologia da Amazônia, Belém, CD-ROM.
Santos, J.O.S., Faria, M.S.G., Riker, S.R., Souza, M.M., Hartmann, L.A., Almeida, M.E., McNaughton, N.J., Fletcher, I.R., 2006b. A faixa colisional K'Mudku (idade Greenvilliana) no norte do Cráton Amazonas: reflexo intracontinental do orógeno Sunsás na margem ocidental do Cráton. In: 9º Simpósio de Geologia da Amazônia, Belém, CD-ROM.
Santos, J.O.S., McNaughton, N.J., Almeida, M.E., 2009. Magmatismo de idade Sunsás no Centro Norte do Cráton Amazonas. XI Simpósio de Geologia da Amazônia. In: 11º Simpósio de Geologia da Amazônia, Manaus, CD-ROM.
Shand, S.J., 1943. Eruptive Rocks: Their Genesis, Composition, Classification, and Their Relation to Ore-deposits with a Chapter on Meteorite. John Wiley & Sons, New York, pp. 488.
Sharp, Z.D., Helffrich, G.R., Bohlen, S.R., Essene, E.J., 1989. The stability of sodalite in the system NaAlSiO4-NaCl. Geochem. Cosmochim. Acta 53, 1943–1954.
Söderlund, U., Johansson, L., 2002. A simple way to extract baddeleyite (ZrO2). G-cubed 3, 1–7.
Söderlund, U., Patchett, P.J., Vervoort, J.D., Isachsen, C.E., 2004. The ^{176}Lu decay constant determined by Lu-Hf and U-Pb isotope systematics of Precambrian mafic intrusions. Earth Planet Sci. Lett. 219, 311–324.
Souza, V.D.S., Souza, A.G.H., Dantas, E.L., Valério, C.D.S., 2015. K'Mudku A-type magmatism in the southernmost Guyana shield, central-north Amazon Craton (Brazil): the case of Pedra do Gavião syenogranite. Braz. J. Genet. 45, 293–306.
Sørensen, H., 1974. The Alkaline Rocks. John Willey & Sons, London, pp. 622.
Sørensen, H., 1992. Agpaitic nepheline syenites: a potential source of rare elements. Appl. Geochem. 7, 417–427.
Sørensen, H., 1997. The agpaitic rocks: an overview. Mineral. Mag. 61, 485–498.
Tassinari, C.C.G., 1996. O Mapa Geocronológico Do Cráton Amazônico No Brasil: Revisão Dos Dados Isotópicos. Habilitation thesis. University of São Paulo, pp. 139.
Tassinari, C.C.G., Macambira, M.J.B., 1999. Geochronological provinces of the amazonian craton. Episodes 22, 174–182.
Tassinari, C.C.G., Macambira, M.J.B., 2004. A evolução tectônica do Cráton Amazônico. In: Neto, V.M., Bartorelli, A., Carneiro, C.D.R., Neves, B.B.B. (Eds.), Geologia do Continente Sul-Americano: Evolução da obra de Fernando Flávio Marques de Almeida. Beca, São Paulo, pp. 471–485.
Teixeira, W., 1978. Significação tectônica do magmatismo anorogênico básico e alcalino na região amazônica. M.S thesis. University of São Paulo, pp. 99.
Tischendorf, G., Förster, H.-J., Gottesmann, B., 2001. Minor- and trace-element composition of trioctahedral micas: a review. Mineral. Mag. 65, 249–276.
Ulbrich, H.H.G.J., Gomes, C.B., 1981. Alkaline rocks from continental Brazil. Earth Sci. Rev. 17, 135–154.
Vaz, P.T., Wanderley Filho, J.R., Bueno, G.V., 2007. Bacia do Tacutu. Bol. Geociencias Petrobras 15, 289–297.
Vendemiatto, M.A., Enzweiler, J., 2001. Routine control of accuracy in silicate rock analysis by X-Ray Fluorescence Spectrometry. Geostand. Geoanal. Res. 25, 283–291.
Wingate, M.T.D., Compston, W., 2000. Crystal orientation effects during ion microprobe U–Pb analysis of baddeleyite. Chem. Geol. 168, 75–97.
Wohlgemuth-Ueberwasser, C.C., Söderlund, U., Pease, V., Nilsson, M.K.M., 2015. Quadrupole LA-ICP-MS U/Pb geochronology of baddeleyite single crystals. J. Anal. At. Spectrom. 30, 1191–1196.